A generic fiber model algorithm for the analysis of arbitrary cross sections under biaxial bending and axial load

Aristotelis Charalampakis and Vlasis Koumousis

Institute of Structural Analysis and Aseismic Research
National Technical University of Athens (NTUA)

Abstract

A generic fiber model algorithm for the analysis of cross sections under biaxial bending and axial load is presented. The method is applied to any cross section (reinforced, composite, repaired etc.) of irregular shape with/without openings and consisting of various materials. The only assumption is that plane sections before bending remain plain after bending (Bernoulli – Euler assumption). The cross section is described by polygons and circles. The material properties are user – defined. The stress – strain diagrams of all materials are composed of any number and any combination of consecutive parabolic or linear parts, subject to a desired accuracy. Various effects such as concrete confinement, concrete tensile strength, strain hardening of the reinforcement etc. may be taken into account, allowing full control of the designer over the entire model. A special purpose computer program with full graphical interface has been developed the main features of which are illustrated in a number of examples.

1. Introduction

The failure of an arbitrary cross-section under biaxial bending and axial load has received extensive attention in the literature lately [1-5]. With the advent of inexpensive computer systems, the generation of the failure surface has been made possible using the "fiber" approach. This approach produces consistent results that agree closely with experimental results [4].

The failure of the cross section corresponds to the top of the moment – curvature diagram. However, the conventional failure, defined by design codes, occurs when any of the materials reaches its predefined maximum allowable strain, either compressive or tensile. Usually, these strains are the yield strains of concrete and steel.

The failure surface is important for non-linear analyses since the plastic deformations of a structural element are functions of the load history and the distance of the load vector from the surface. Moreover, it provides grounds for a damage analysis for the cross section.

2. Generation of failure surface

There are three different techniques to generate the failure surface of an arbitrary cross section: (1) interaction curves for a given bending moments ratio, (2) load contours for a given axial load and (3) isogonic or 3D curves.

The first two techniques require the calculation of the position of the neutral axis. The set of equilibrium equations are non linear and coupled, and an iterative approach such as the quasi-Newton method proposed by Yen [6], is needed to determine the position of the neutral axis. These procedures are not straightforward to implement and, in many cases, are sensitive to the selection of the origin of the reference system. These algorithms usually become unstable near the state of pure compression.

On the other hand, the third technique, which is used in the method presented, is more direct because the direction of the neutral axis is assumed from the very beginning. The produced points describe a more complex 3D plot, because the meridians, in general, are not plane. This is due to the asymmetry of the cross section, as described later.

3. Cross Section

The cross section is described by polygons and circles. Arcs are approximated by polygon chains to a specified accuracy. All graphical objects must not intersect.

Importing a cross section from a DXF file may produce the following:

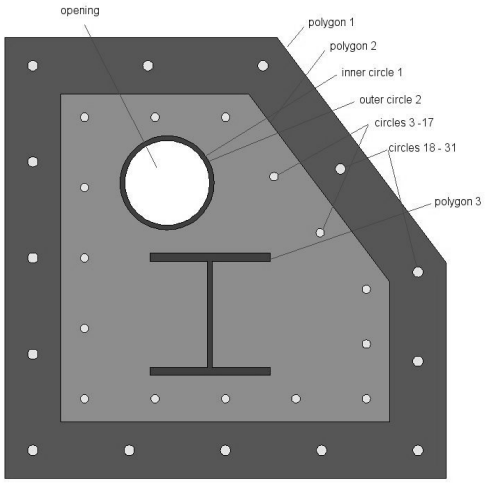

All graphical objects have two material properties: the “foreground” material and the “background” material. The foreground material is taken into account with a positive sign during the calculation of the stress resultants, whereas the background material is taken into account with a negative sign. In this way, complex cross sections may be described easily, by assigning the correct layer of each graphical object. In the previous example, the material properties are set as follows:

Object	Foreground material	Background material
Polygon 1	Unconfined (outer) concrete	None
Polygon 2	Confined (inner) concrete	Unconfined (outer) concrete
Polygon 3	Structural steel	Confined (inner) concrete
Circle 1	None	Structural steel
Circle 2	Structural steel	Confined (inner) concrete
Circles 3 - 17	Reinforcement	Confined (inner) concrete
Circles 18 - 31	Reinforcement	Unconfined (outer) concrete

4. Materials

The stress – strain diagrams of all materials are composed of any number and any combination of consecutive parabolic or linear segments. The parabolic segments are defined by three consecutive points, i.e. an intermediate point in addition to the end points. The intermediate point need not be in the middle. For example, the stress strain diagram of a certain kind of steel may be as follows:

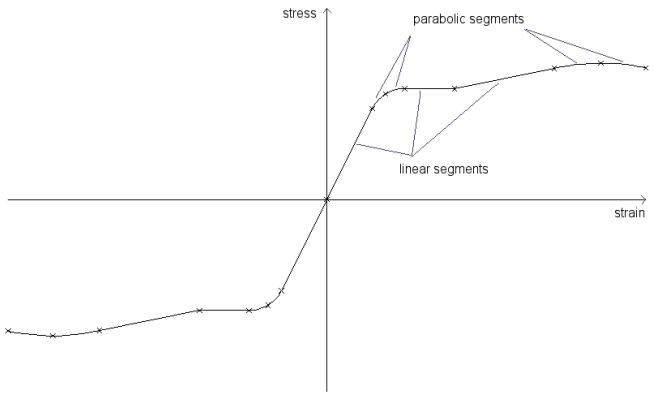

Apart from the stress – strain diagram, the material structure holds data related to the maximum compressive and tensile strain and whether reach of these values signifies the conventional failure of the cross section.

5. Calculations

The combination of polygons and circles covers almost all cases of arbitrary defined cross sections. Arcs may be approximated by a series of straight lines; however, if the arc is not significant, as is the case of small radius fillets between lines, it is recommended that it is approximated by a single straight line.

Any convenient point may be used as origin for the calculations. Since the direction of the neutral axis is assumed from the beginning, it is convenient to express all coordinates to another YZ Cartesian system with the Y axis parallel to the neutral axis. Therefore, the cross section is rotated around the origin by an angle $-\theta$, as shown in fig 5.1, by a simple rotational transformation, expressed by (5.1).

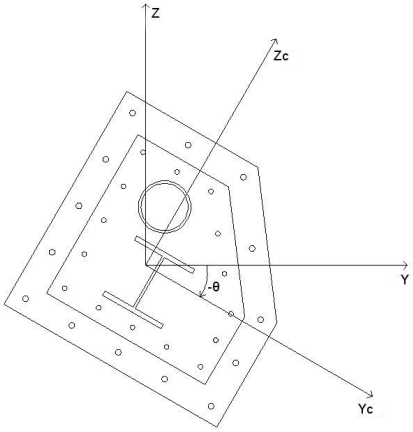

Fig. 5.1. Rotation around the origin

$$\begin{bmatrix} Y \\ Z \end{bmatrix} = \begin{bmatrix} \cos(\theta) & -\sin(\theta) \\ \sin(\theta) & \cos(\theta) \end{bmatrix} \cdot \begin{bmatrix} Y_c \\ Z_c \end{bmatrix} \tag{5.1}$$

Since the direction of the neutral axis is assumed, the stresses vary only in the Z axis.

The next step is the trapezoidal decomposition of all polygons, which is accomplished using the "plane sweep algorithm". The trapezoids are parallel to the neutral axis. This procedure needs to be done only once for each assumed direction of the neutral axis; this basic set of trapezoids may be stored and retrieved when needed. For example, the steel section will be decomposed as shown in fig 5.2.

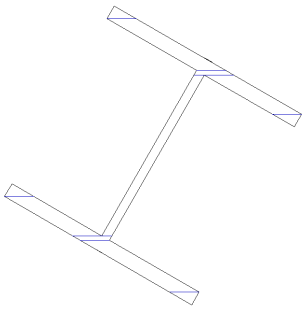

Fig. 5.2. Trapezoidal decomposition of a steel section.

The strain distribution over the cross section is controlled by two variables i.e. the strain ε_c at the origin and the curvature k; therefore, the strain at each point at the cross section is given by (5.2).

$$\varepsilon = \varepsilon_c + k \cdot z \tag{5.2}$$

For the calculation of the stress resultants produced by a certain material, the exact z coordinates of the transition points i.e. the points between linear and / or parabolic parts of the stress – strain diagram, can be calculated. The basic set of trapezoids is now further decomposed into smaller trapezoids, based on these coordinates. Furthermore, the circles are decomposed into strips parallel to the Y axis.

The stress resultants for the trapezoids are then calculated as follows (fig. 5.3):

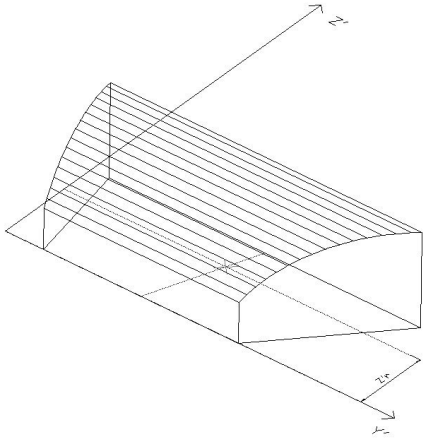

Fig. 5.3. Calculation of stress resultants for a trapezoid

The force and the coordinate z_r' of the centroid are calculated by integration of the stress diagram along the Z' axis. The y_r' coordinate of the stress resultant can be found geometrically, as it is the intersection point of the median connecting the top and bottom sides of the trapezoid and the horizontal line at distance z_r' from the bottom fiber.

The width of the trapezoid can be expressed as a function of z' (eq. 5.3). Also, we assume that the stress distribution over the trapezoid is parabolic, which is the general case (eq. 5.4).

$$l = a_{1l} \cdot z' + a_{0l} \tag{5.3}$$

$$\sigma = a_{2\sigma} \cdot z'^2 + a_{1\sigma} \cdot z' + a_{0\sigma} \tag{5.4}$$

The force, moment around the Y' axis and the z_r' coordinate of the centroid are given by equations (5.5).

$$\begin{aligned} F &= \frac{1}{4} a_{2\sigma} \cdot a_{1l} \cdot h^4 + \frac{1}{3} a_{1\sigma} \cdot a_{1l} \cdot h^3 + \frac{1}{3} a_{2\sigma} \cdot a_{0l} \cdot h^3 + \frac{1}{2} a_{0\sigma} \cdot a_{1l} \cdot h^2 + \\ &+ \frac{1}{2} a_{1\sigma} \cdot a_{0l} \cdot h^2 + a_{0\sigma} \cdot a_{0l} \cdot h \\ M_{Y'} &= \frac{1}{5} a_{2\sigma} \cdot a_{1l} \cdot h^5 + \frac{1}{4} a_{1\sigma} \cdot a_{1l} \cdot h^4 + \frac{1}{4} a_{2\sigma} \cdot a_{0l} \cdot h^4 + \frac{1}{3} a_{0\sigma} \cdot a_{1l} \cdot h^3 + \\ &+ \frac{1}{3} a_{1\sigma} \cdot a_{0l} \cdot h^3 + \frac{1}{2} a_{0\sigma} \cdot a_{0l} \cdot h^2 \\ z_r' &= M_{Y'} \Big/ F \end{aligned} \tag{5.5}$$

Similarly, the stress resultants for the circles are calculated as follows (fig. 5.4):

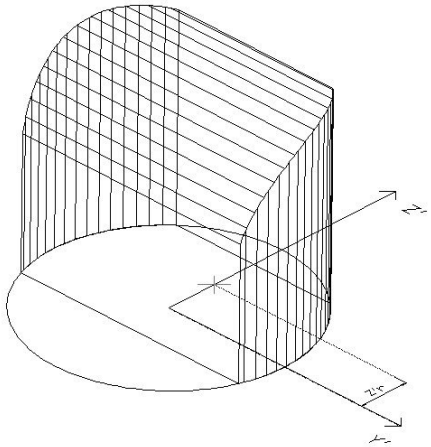

Fig. 5.4. Calculation of stress resultants for a circular section

The force and the coordinate z_r' of the centroid are calculated by integration of the stress diagram along the Z' axis. The stress resultant lies on the Z' axis due to symmetry.

The width can be expressed as a function of z' (eq. 5.6). As previously, we assume that the stress distribution over the trapezoid is parabolic, which is the general case (eq. 5.4).

$$l = 2 \cdot \sqrt{R^2 - z'^2} \tag{5.6}$$

where, R is the radius of the circle. Assuming that the z' coordinates of the bottom and top fiber are z_1' and z_2' respectively, the force, moment around the Y' axis and the z_r' coordinate of the centroid are given by equations (5.7).

$$\begin{aligned}
F &= \frac{1}{12}\left(6 \cdot a_{2\sigma} \cdot z_1' + 8 \cdot a_{1\sigma}\right) \cdot \sqrt[3]{R^2 - z_1'^2} - \frac{1}{12}\left(6 \cdot a_{2\sigma} \cdot z_2' + 8 \cdot a_{1\sigma}\right) \cdot \sqrt[3]{R^2 - z_2'^2} + \\
&+ \frac{1}{4}\left(z_2' \cdot \sqrt{R^2 - z_2'^2} - z_1' \cdot \sqrt{R^2 - z_1'^2} - R^2 \cdot \left(ArcSin\left(\frac{z_1'}{R}\right) - ArcSin\left(\frac{z_2'}{R}\right)\right)\right) \cdot \\
&\cdot \left(a_{2\sigma} \cdot R^2 + 4 \cdot a_{0\sigma}\right) \\
M_{Y'} &= \frac{1}{60}\left(16 \cdot a_{2\sigma} \cdot R^2 + 40 \cdot a_{0\sigma} + 24 \cdot a_{2\sigma} \cdot z_1'^2 + 30 \cdot a_{1\sigma} \cdot z_1'\right) \cdot \sqrt[3]{R^2 - z_1'^2} - \\
&- \frac{1}{60}\left(16 \cdot a_{2\sigma} \cdot R^2 + 40 \cdot a_{0\sigma} + 24 \cdot a_{2\sigma} \cdot z_2'^2 + 30 \cdot a_{1\sigma} \cdot z_2'\right) \cdot \sqrt[3]{R^2 - z_2'^2} - \\
&- \frac{1}{4} \cdot a_{1\sigma} \cdot \left(z_1' \cdot \sqrt{R^2 - z_1'^2} - z_2' \cdot \sqrt{R^2 - z_2'^2} + R^2 \cdot \left(ArcSin\left(\frac{z_1'}{R}\right) - ArcSin\left(\frac{z_2'}{R}\right)\right)\right) \cdot R^2 \\
z_r' &= M_{Y'} \Big/ F
\end{aligned}$$

(5.7)

6. Construction of moment – curvature diagram

For given values of axial load and angle θ, small increments $\Delta\varphi$ are applied as imposed curvature. Since the curvature k of eq. 5.2 is given, the algorithm uses a fast Newton – Raphson method to calculate the strain ε_c at the centroid in order to achieve axial equilibrium to a specified accuracy.

As the curvature increases, the neutral axis moves perpendicular to its direction. This incremental procedure continues until the primary moment diagram reaches a maximum (failure) or until one of the materials reaches the maximum compressive or tensile strain specified by the user (conventional failure). Thus, the complete moment – curvature diagram can be obtained, both for the primary moment M_y and for secondary moment M_z.

The algorithm uses a variable curvature step; therefore, the final result is independent of the initial curvature step (specified by the user). A small initial curvature step produces a smooth moment – curvature diagram.

Finally, the moments can be expressed in the global reference system with a rotational transformation (eq. 6.1).

$$\begin{bmatrix} M_{YC} \\ M_{ZC} \end{bmatrix} = \begin{bmatrix} \cos(\theta) & \sin(\theta) \\ -\sin(\theta) & \cos(\theta) \end{bmatrix} \cdot \begin{bmatrix} M_Y \\ M_Z \end{bmatrix} \tag{6.1}$$

7. Construction of failure surfaces

By repeating the procedure described previously for different directions θ of the neutral axis in the range of $0 – 359^0$, we are able to construct the failure surfaces equator by equator.

8. Computer implementation

A computer program, called myBiAxial, which implements the method presented, has been developed. The program features a full graphical interface. It is also capable of importing cross sectional data from DXF files. Some screenshots are the following:

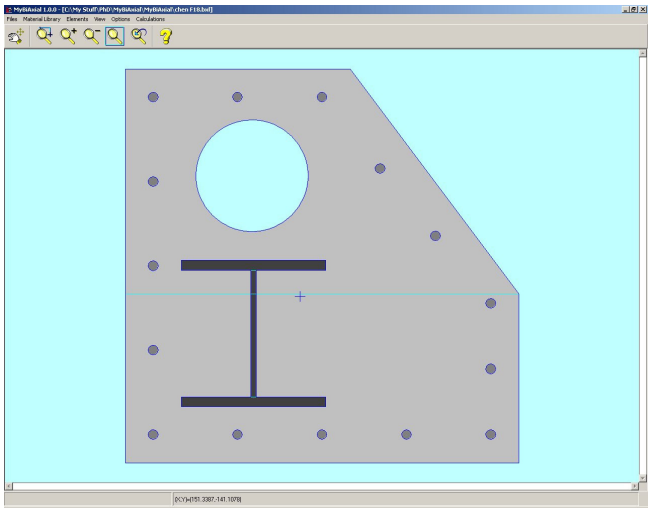

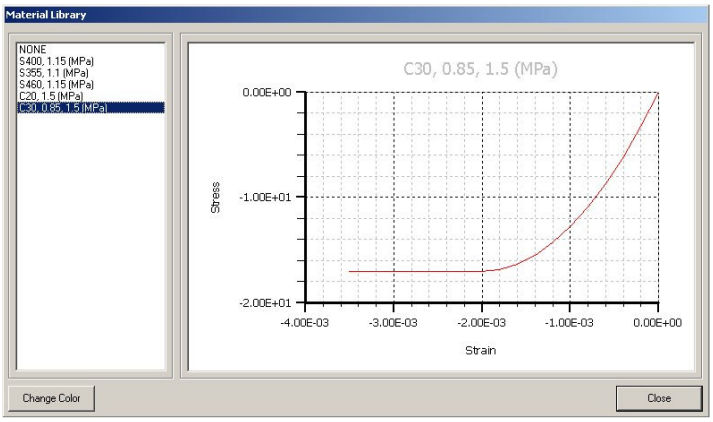

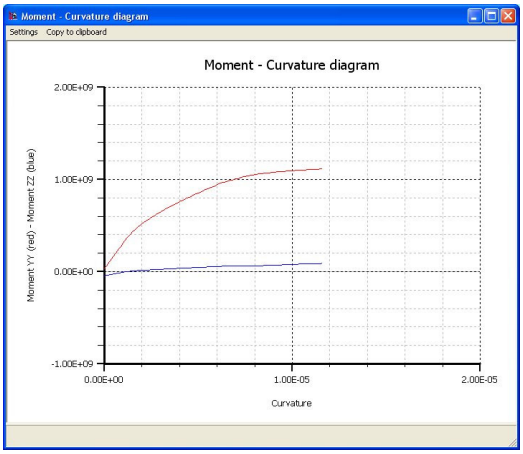

9. Validation – examples

9.1 Example 1

Eurocode 2 provides design charts for common reinforced concrete cross sections. These charts provide combinations of axial loads and their respective ultimate bending moment capacities (which correspond to the conventional failure of the cross section), for a range of longitudinal reinforcement expressed by the mechanical reinforcement percentage ω (eq. 9.1.1).

$$\omega = \frac{A_{s,tot}}{A_{c,tot}} \cdot \frac{f_{yd}}{f_{cd}} \tag{9.1.1}$$

where $A_{s,tot}$ is the total area of longitudinal reinforcement, $A_{c,tot}$ is the total area of concrete, f_{yd}, f_{cd} are the design strengths of steel and concrete respectively. Also, the axial load and bending moment are normalized with respect to the concrete properties and the cross sectional dimensions (eq. 9.1.2); therefore, a single chart covers all cases for a certain steel grade.

$$\begin{aligned} \nu &= \frac{N_d}{A_{c,tot} \cdot f_{cd}} \\ \mu &= \frac{M_d}{A_{c,tot} \cdot h \cdot f_{cd}} \end{aligned} \tag{9.1.2}$$

Eurocode 2 specifies the value of 0.020 as the ultimate strain limit for longitudinal steel reinforcement. Also, for large compressive axial loads, it reduces the ultimate curvature capacity by imposing the rotation of the strain profile around point C which is located at a distance $\frac{3}{7}h$ from the most compressed fiber and has a strain of $\varepsilon_0 = -0.002$. This restriction is included easily in the algorithm; however, it is of little practical interest since large compressive axial loads in concrete cross sections must be avoided for other reasons i.e. creep.

The developed computer program was used to calculate pairs of axial loads and bending moments for the rectangular cross section of fig. 9.1.1(a). The characteristic strengths and partial safety factors for concrete and reinforcement bars were taken as follows:

$$\begin{aligned} f_{ck} &= 20MPa, \gamma_c = 1.5 \\ f_y &= 500MPa, \gamma_r = 1.15 \end{aligned}$$

Five different cases of longitudinal reinforcement were considered, i.e. $\omega = 0.00,\ 0.50,\ 1.00,\ 1.50,\ 2.00$. The corresponding design chart is shown in fig. 9.1.2(b).

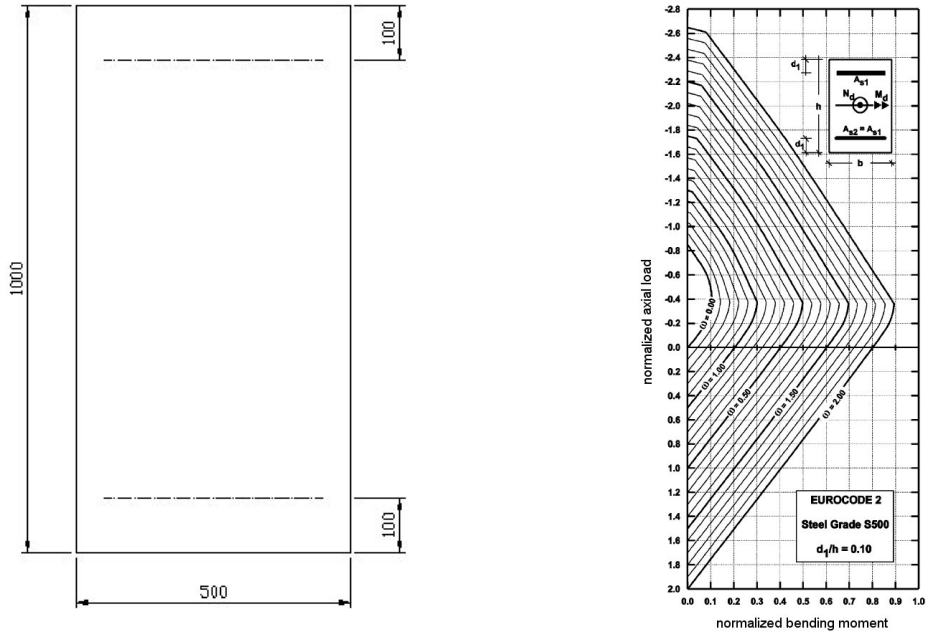

(a) (b)

Fig. 9.1.1. (a) Rectangular reinforced concrete cross section (distances in mm) (b) Corresponding Eurocode 2 design chart (steel grade S500)

The computed results, summarized in table 9.1.1, follow the corresponding ω curve exactly, as shown in fig. 9.1.2.

v	$\mu\ (\omega = 0)$	$\mu\ (\omega = 0.50)$	$\mu\ (\omega = 1.00)$	$\mu\ (\omega = 1.50)$	$\mu\ (\omega = 2.00)$
1.60					0.1607
1.40				0.0402	0.2408
1.20				0.1203	0.3219
1.00				0.2007	0.4031
0.80			0.0801	0.2823	0.4841
0.60			0.1613	0.3636	0.5645
0.40		0.0400	0.2433	0.4440	0.6441
0.20		0.1228	0.3237	0.5232	0.7230
0.00	0.0000	0.2031	0.4020	0.6015	0.8016
-0.10	0.0424	0.2412	0.4406	0.6402	0.8397
-0.20	0.0746	0.2748	0.4739	0.6728	0.8717
-0.30	0.0951	0.2939	0.4920	0.6903	0.8883
-0.35	0.1010	0.2988	0.4967	0.6944	0.8919
-0.40	0.1033	0.2943	0.4883	0.6828	0.8775
-0.60	0.0824	0.2465	0.4287	0.6176	0.8091
-0.80	0.0193	0.1938	0.3690	0.5526	0.7409
-1.00		0.1292	0.3072	0.4875	0.6729
-1.20		0.0548	0.2406	0.4214	0.6047
-1.40			0.1670	0.3525	0.5358
-1.60			0.0897	0.2792	0.4652
-1.80				0.2030	0.3921

-2.00				0.1245	0.3159
-2.20					0.2384
-2.40					0.1595

Table. 9.1.1. Computed results

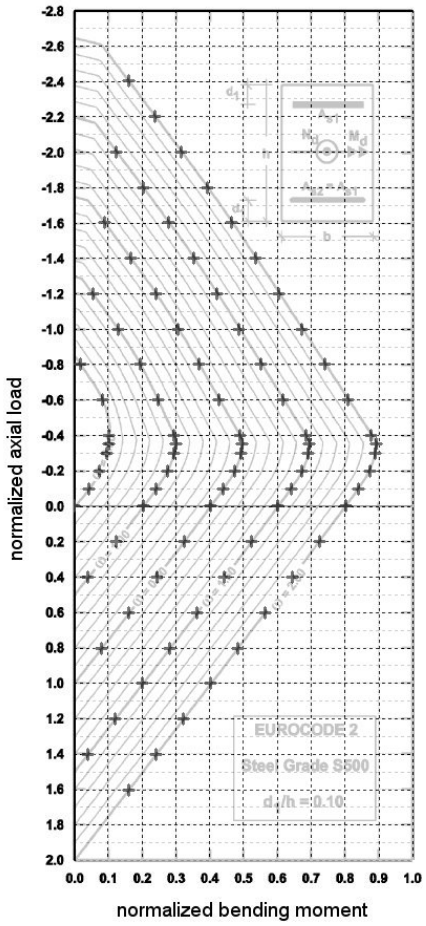

Fig. 9.1.2. Computed results superimposed over the EC2 design chart

9.2 Example 2

This is an example presented by Chen et al. [4], which invokes the polygonal composite column cross section of figure 9.2.1. The cross section consists of a concrete core, an asymmetrically placed H – shaped steel section, 15 reinforcement bars of diameter 18mm and a circular opening.

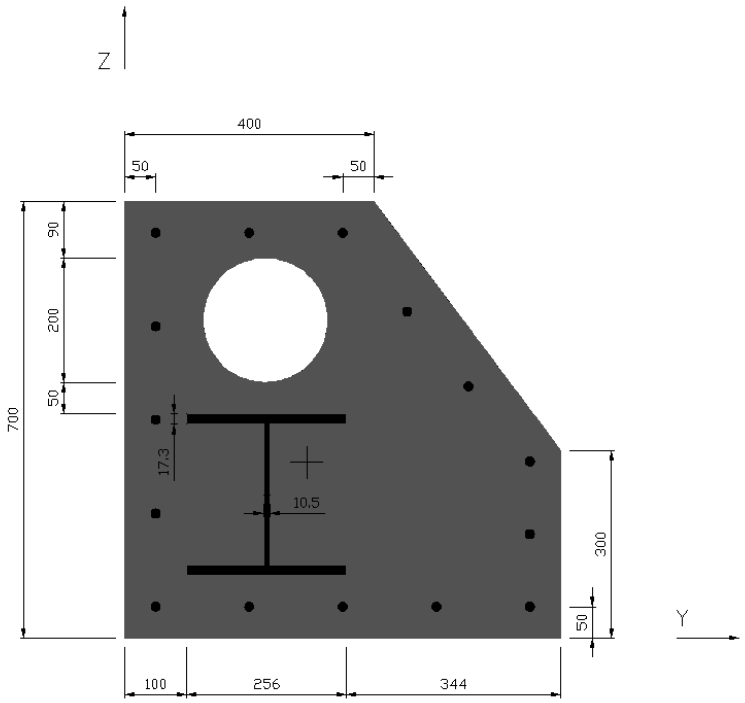

Fig. 9.2.1. Composite column cross section

Chen et al. use a quasi – Newton method [6] to analyze the cross section. However, the convergence of the iterative process invoked by the algorithm cannot be guaranteed when dealing with large axial loads i.e. loads that approach the axial load capacity under pure compression. In order to ensure the stability of the algorithm, the plastic centroid must be used as the origin of the Cartesian system. For an arbitrary cross section, the plastic centroid can be calculated as follows:

$$Y_{pc} = \frac{Y_c \cdot A_c \cdot f_{cc} / \gamma_c + Y_s \cdot A_s \cdot f_s / \gamma_s + Y_r \cdot A_r \cdot f_r / \gamma_r}{A_c \cdot f_{cc} / \gamma_c + A_s \cdot f_s / \gamma_s + A_r \cdot f_r / \gamma_r}$$
$$Z_{pc} = \frac{Z_c \cdot A_c \cdot f_{cc} / \gamma_c + Z_s \cdot A_s \cdot f_s / \gamma_s + Z_r \cdot A_r \cdot f_r / \gamma_r}{A_c \cdot f_{cc} / \gamma_c + A_s \cdot f_s / \gamma_s + A_r \cdot f_r / \gamma_r} \qquad (9.2.1)$$

where, A_c, A_r, A_s are the total areas of concrete, reinforcing bars and structural steel respectively; f_{cc}, f_r, f_s are the respective characteristic strengths; γ_{cc}, γ_r, γ_s are the respective partial safety factors, Y_c, Z_c, Y_r, Z_r, Y_s, Z_s, are the coordinates of the respective centroids. In this case, the coordinates of the plastic centroid with respect to the bottom left corner are [4]:

$$Y_{pc} = 292.2mm,\ Z_{pc} = 281.5mm$$

The stress – strain curve for concrete (CEC 1994) which consists of a parabolic and a linear (horizontal) part was used in the calculation, with $f_{cc} = 0.85 \cdot f_{ck} / \gamma_c$, $\varepsilon_0 = 0.002$

and $\varepsilon_{cu} = 0.0035$. The Young modulus for all steel sections was 200GPa while the maximum strain was $\varepsilon_u = \pm 0.010$.

The characteristic strengths and partial safety factors for concrete, structural steel and reinforcement bars were taken as follows:

$$f_{ck} = 30MPa, \gamma_c = 1.5$$
$$f_s = 355MPa, \gamma_s = 1.1$$
$$f_y = 460MPa, \gamma_r = 1.15$$

The analysis was carried out with an angle step of 5 degrees.

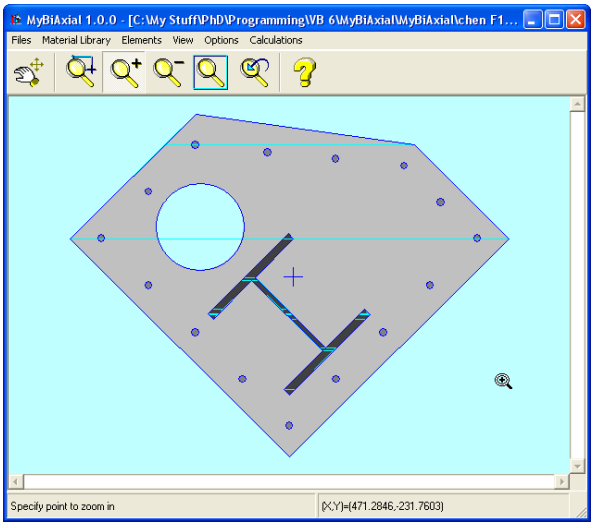

Fig. 9.2.2. Example 9.2 in MyBiAxial

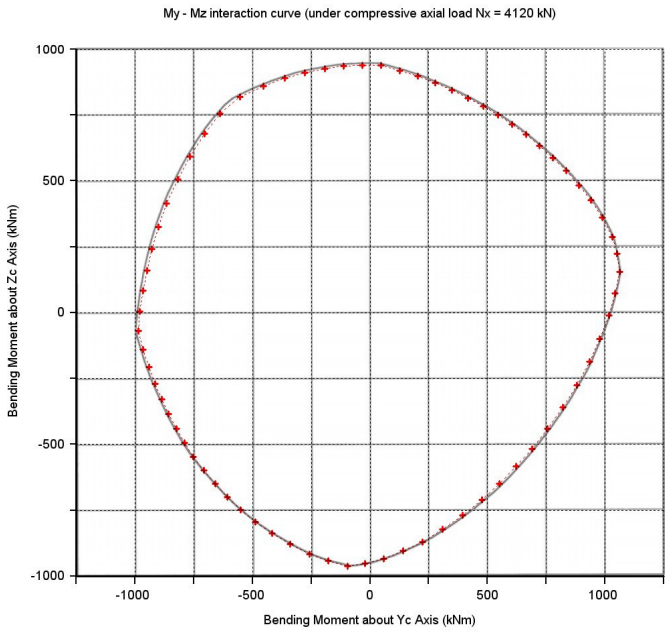

Fig. 9.2.3. M_{Yc} - M_{Zc} interaction curve for compressive axial load N_X=4120KN

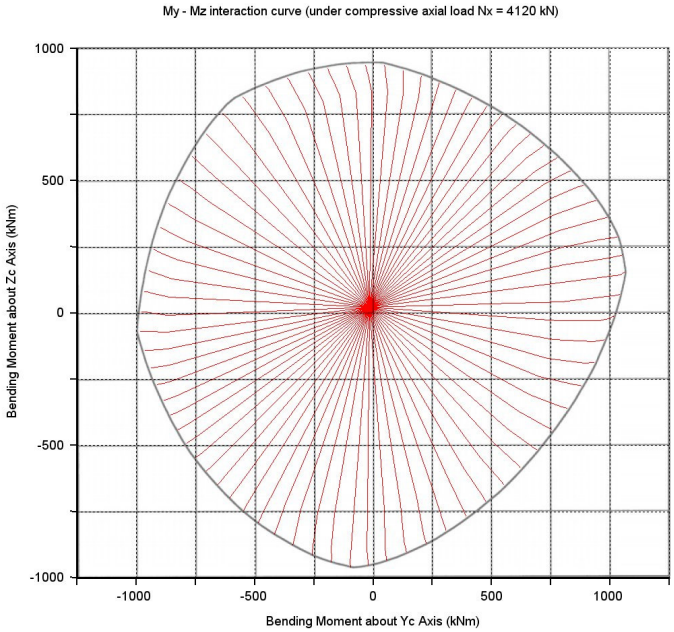

Fig. 9.2.4. M_{Yc} - M_{Zc} interaction curve for compressive axial load N_X=4120KN, showing the full path for each analysis.

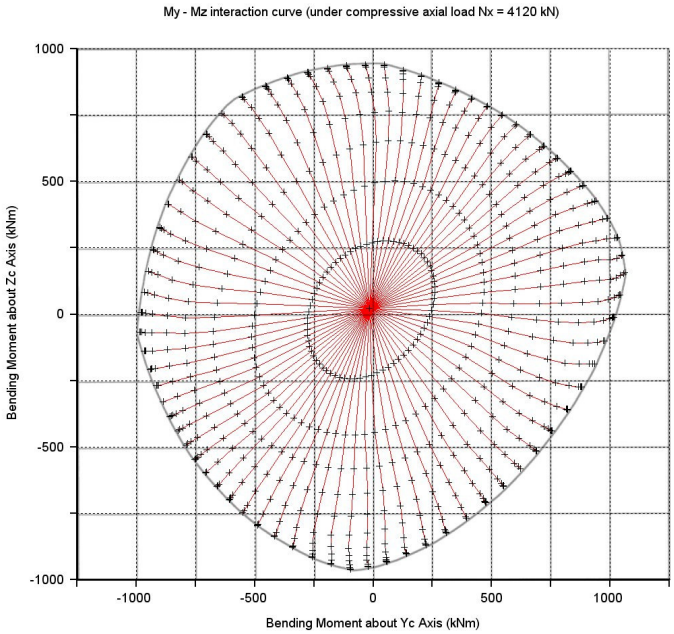

Fig. 9.2.5. M_{Yc} - M_{Zc} interaction curve for compressive axial load N_X=4120KN, with an initial curvature step of 1.0E-06.

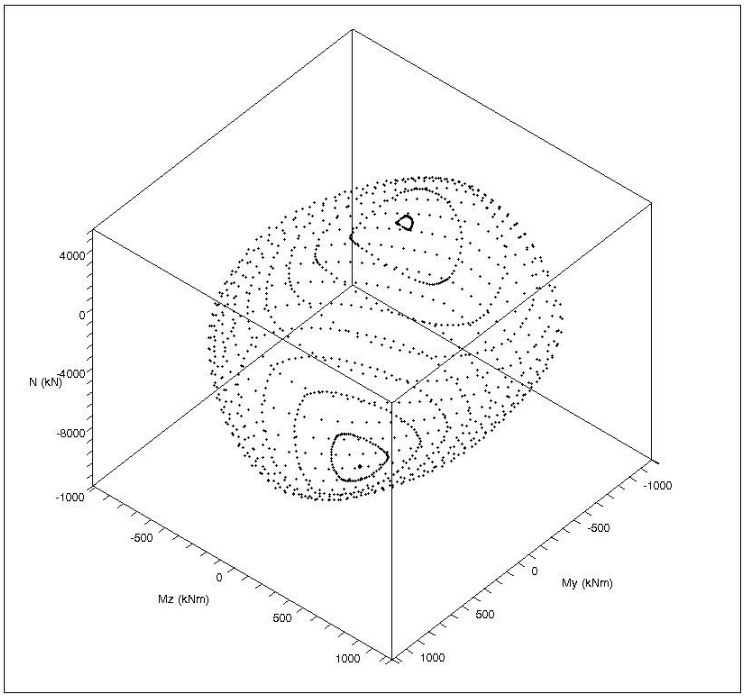

Fig. 9.2.6. Complete conventional failure surface.

Figure 9.2.3 shows the results of this method superimposed over the results taken from [4].

Figure 9.2.4 shows the full path for each analysis. Each spike is produced as the angle of the neutral axis is increased by 5 degrees. The spikes are not straight lines because of the secondary moment M_{zz} which, in turn, is related to the asymmetry of the cross section. The ends of the spikes represent the conventional failure of the cross section.

In addition, figure 9.2.5 shows the results for each analysis as scattered data. The analysis took place with an initial curvature step of 1.0E-06 and a maximum axial load error of 1N. The algorithm automatically decreases the curvature step if the new curvature cannot be applied; therefore the scattered data become increasingly dense near the conventional failure i.e. the contour itself.

Finally, figure 9.2.6 shows the complete conventional failure surface.

9.3 Example 3

In this example, the versatility of the proposed algorithm is demonstrated. The task is to check the maximum bending moment capacity of a bolted connection of two circular tubes of diameter/width 1520/22mm and 1400/12.7mm respectively. The connection is implemented by means of two circular flanges and 24 bolts arranged in circle. The flanges are reinforced externally by dense out – of – plane triangular steel elements, as shown in the figures.

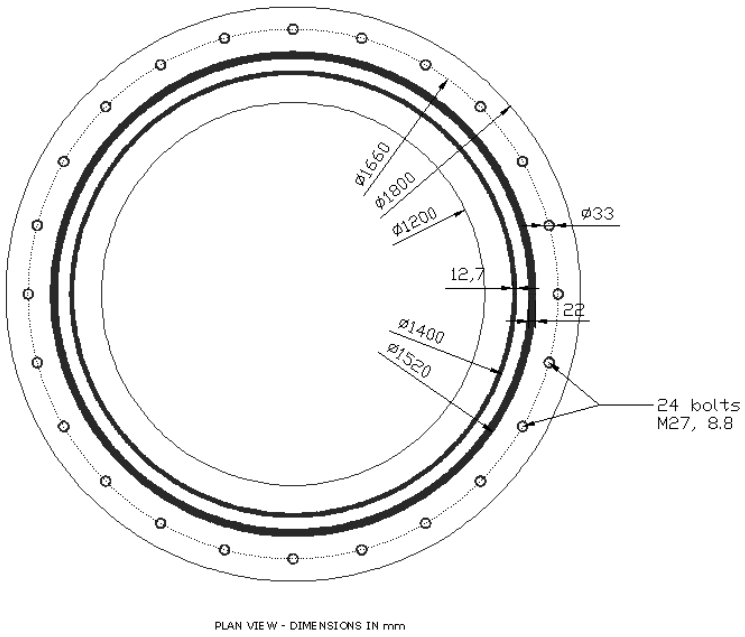

Fig. 9.3.1. Plan view of the proposed connection.

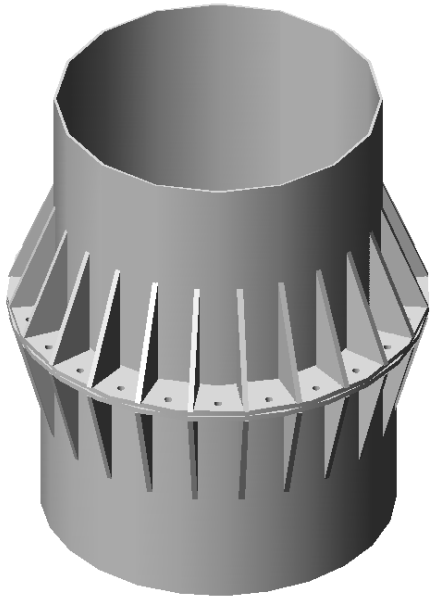

Fig. 9.3.2. 3d view of the proposed connection.

Bottom tube, external diameter	1520mm
Bottom tube, thickness	22mm
Top tube, external diameter	1400mm
Top tube, thickness	12.7
Flange, external diameter	1800mm
Flange, internal diameter	1200mm
Flange, thickness	25mm
Steel grade	FE360

Number of bolts	24
Bolt size	M27
Bolt quality	8.8
Bolts arrangement, circle diameter	1660mm
Bolts hole, circle diameter	33mm (3mm tolerance)
Axial load (compressive)	325kN

Table 9.3.1. Properties.

We assume that the flanges are rigid by virtue of the triangular steel elements. However, the rigidity does not extend to the inner circle of the two flanges; we assume that the effective rigid ring has a width of 187mm, as shown in fig. 9.3.3.

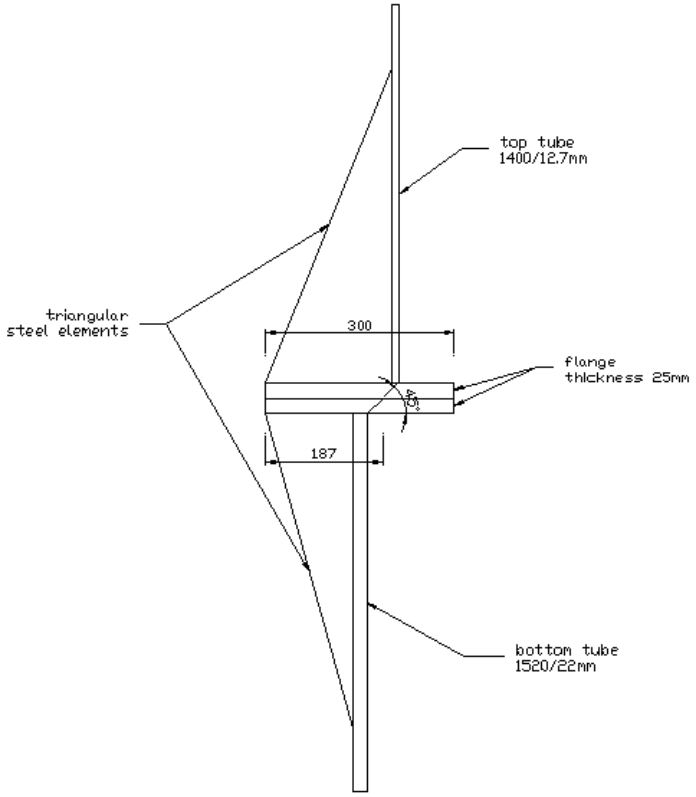

Fig. 9.3.3. Section of the proposed connection.

Two materials are now defined: the flanges (steel grade Fe360) behave linearly in compression up to yield strength i.e. $^{235MPa}/_{1.10} = 213.636MPa$; however they do not exhibit tensile strength (fig. 9.3.4). We expect the flanges not to yield i.e. the failure should occur because of the bolts.

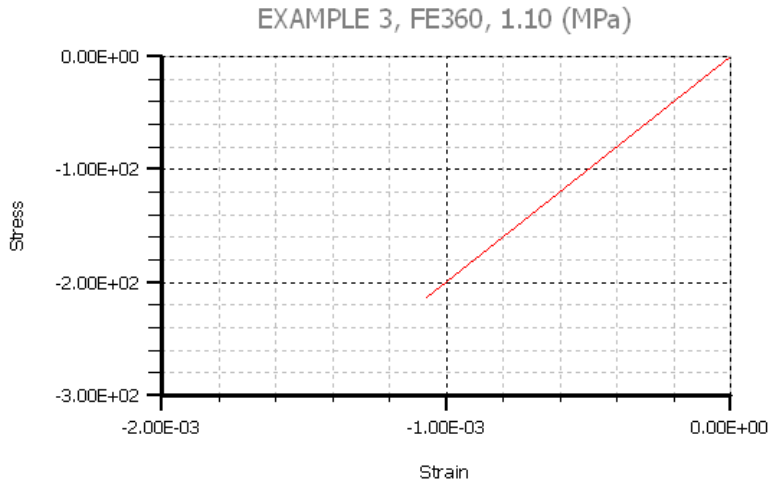

Fig. 9.3.4. Flange material in myBiAxial.

We assume that the bolts (quality 8.8) exhibit a bilinear behaviour. The first linear segment extends in tension up to yield strength i.e. $640MPa/1.25 = 512MPa$; the second linear segment extends up to ultimate strength defined by Eurocode 3, i.e. $0.9 \cdot 800MPa/1.25 = 576MPa$; however they do not exhibit compressive strength (fig. 9.3.5).

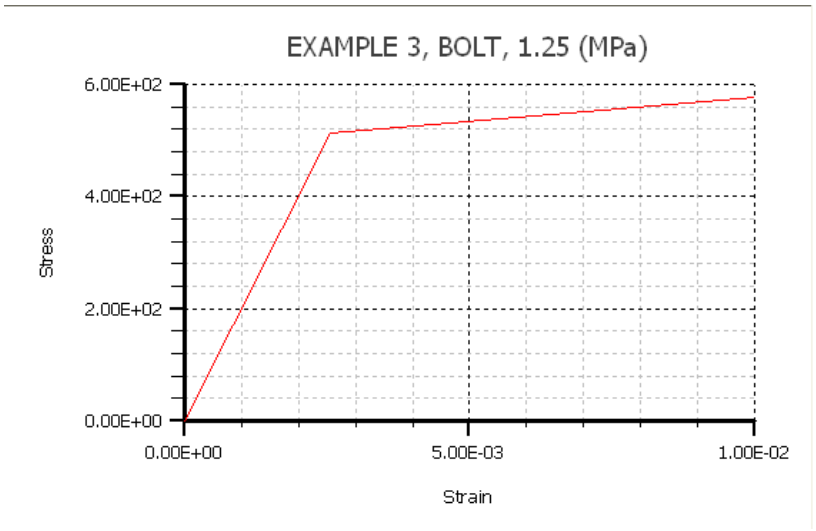

Fig. 9.3.5. Bolt material in myBiAxial.

Young modulus is taken equal to $200GPa$ for all cases. Of course, the material properties may be defined otherwise and may also include parabolic segments, subject to the user's needs or assumptions.

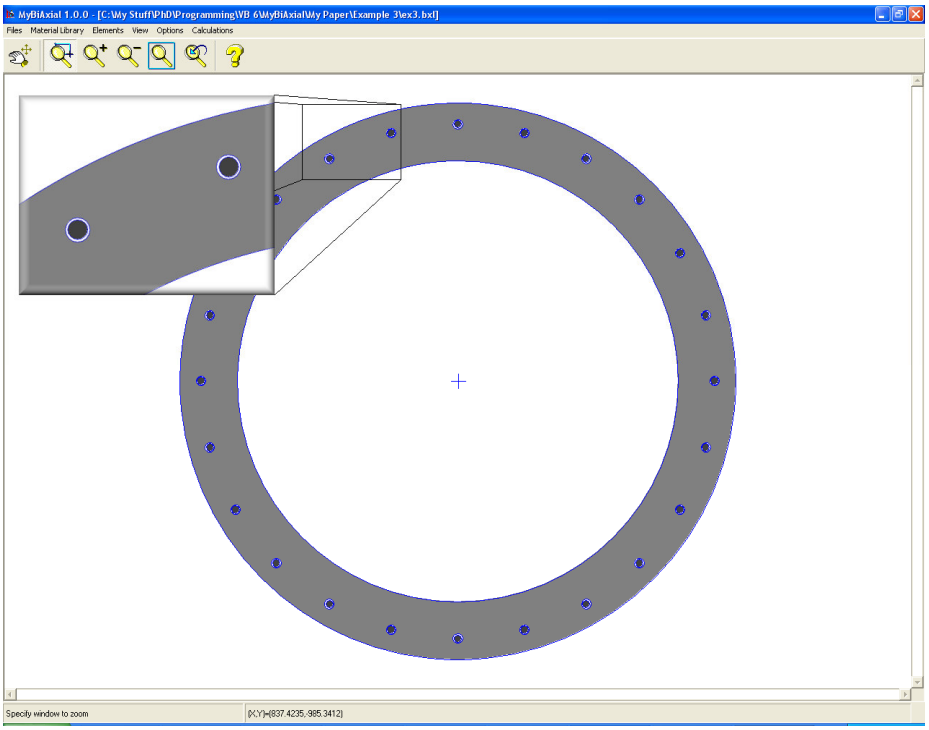

Fig. 9.3.6. Example 3 in my BiAxial.

For an axial (compressive) load of $N_{Xc} = 325kN$, the algorithm yields the following results: curvature $k = 6.223 \cdot 10^{-6}$, strain at the origin $\varepsilon_c = 4.751 \cdot 10^{-3}$, ultimate bending moment at failure $M_{Yc} = 6466.160kNm$. The minimum strain for the flanges is $\varepsilon_{\min,flanges} = -8.493 \cdot 10^{-4}$; therefore, the flanges do not yield, as assumed from the beginning. The failure occurs because of the outermost bolt, which reaches the maximum strain of $\varepsilon_{\max,bolts} = +0.010$.

Based on these data, the stress solids were created using CAD software (fig. 9.3.7). The results are summarized in table 9.3.2; the sum of the volume of all stress solids is equal to the axial load and the sum of all moments is equal to the result obtained from the proposed algorithm.

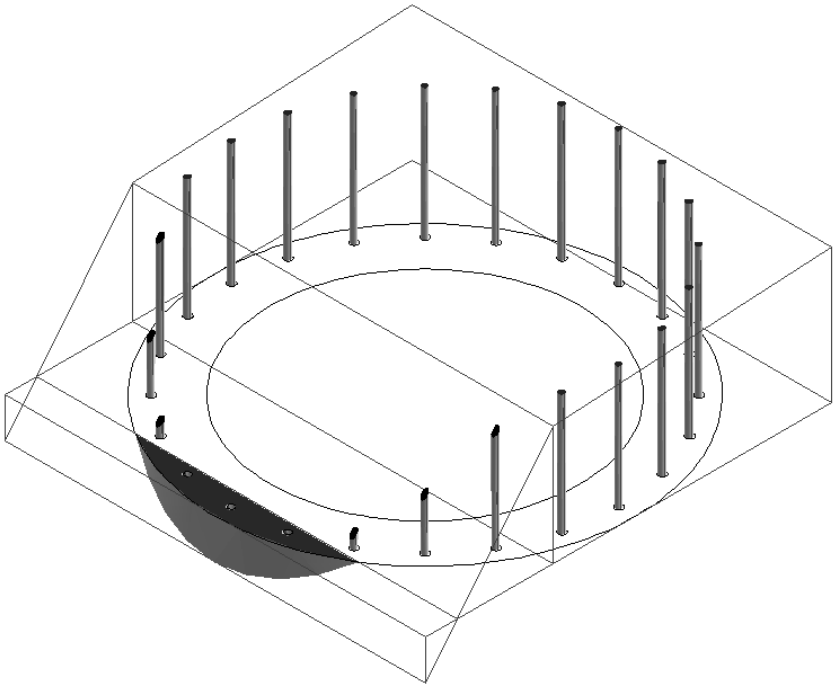

Fig. 9.3.7. Stress solids with CAD software.

Element	Volume (or Force, kN)	Y_c Coordinate of Centroid (mm)	Bending Moment M_{Yc} (kNm)
Flange	-5876.256622	-842.4518	4950.462969
Bolts #11 (x 2)	63.7177013	-717.782	-45.73541907
Bolts #10 (x 2)	251.6976392	-586.6406	-147.6560541
Bolts #9 (x 2)	496.6778638	-414.8693	-206.0563977
Bolts #8 (x 2)	594.7123633	-214.8151	-127.7531958
Bolts #7 (x 2)	607.8800651	0	0
Bolts #6 (x 2)	621.0477669	214.8243	133.4161518
Bolts #5 (x 2)	633.3181116	415.0044	262.8298029
Bolts #4 (x 2)	643.8548955	586.903	377.8803697
Bolts #3 (x 2)	651.9400541	718.8054	468.6180314
Bolts #2 (x 2)	657.0225973	801.7227	526.7499307
Bolt #1 (x 1)	329.378079	830.0042	273.385189
Sums :	-325.0094853		6466.141378

Table 9.3.2. Results obtained from CAD software.

As expected, the interaction curve, shown in figure 9.3.8, is symmetrical. Note that since the secondary moment M_z is zero at all times, the paths of all analyses are straight lines.

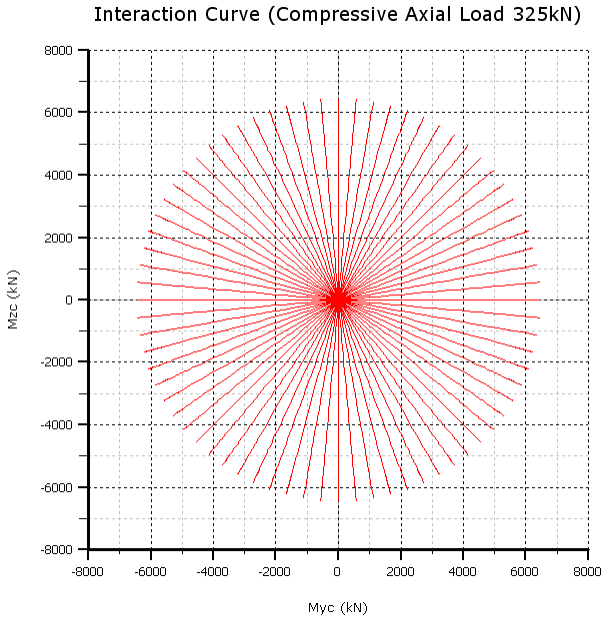

Fig. 9.3.8. Interaction curve for compressive axial load N_x = 325kN.

9.4 Example 4

In this example, the task is to calculate the maximum bending moment capacity of a rigid footing (fig. 9.4.1.). We assume that the footing is placed over sand modeled with independent springs (Winkler); failure occurs when stress exceeds a predefined maximum value.

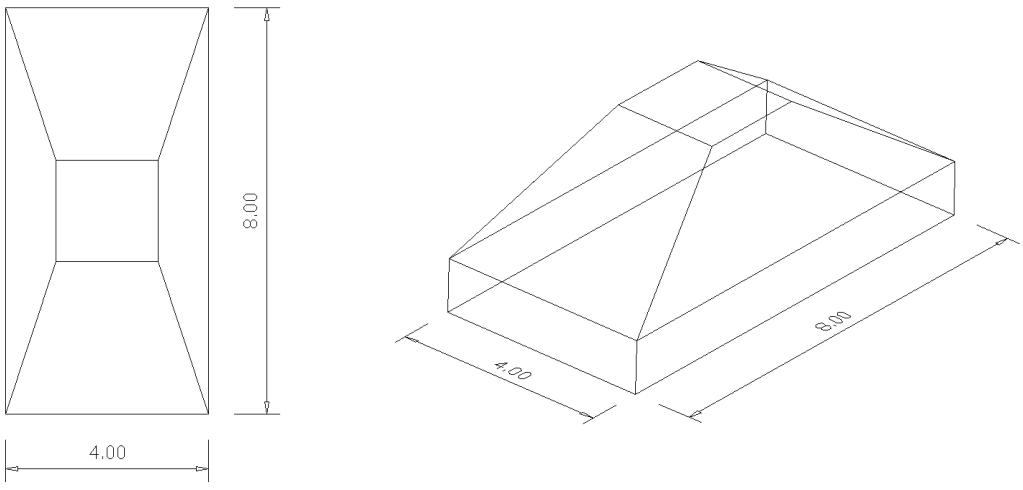

Fig. 9.4.1. Rigid footing (distances in m) (a) Plan view (b) 3D view

Rigid footing, length	8.00m
Rigid footing, width	4.00mm
Axial load (compressive)	1300kN

Sand, k	20KPa / mm
Sand, maximum stress	250KPa

Table 9.4.1. Properties.

We assume that sand behaves linearly in compression up to a maximum stress of $250KPa$ with a subgrade modulus $k_s = {20KPa}/{mm}$ (maximum settlement is $12.5mm$); also, it does not exhibit tensile strength (fig. 9.3.2). Note that linear behavior is not obligatory; the algorithm can handle parabolic segments as well as linear segments. Also, in this case, the stresses are expressed with respect to settlement instead of strain.

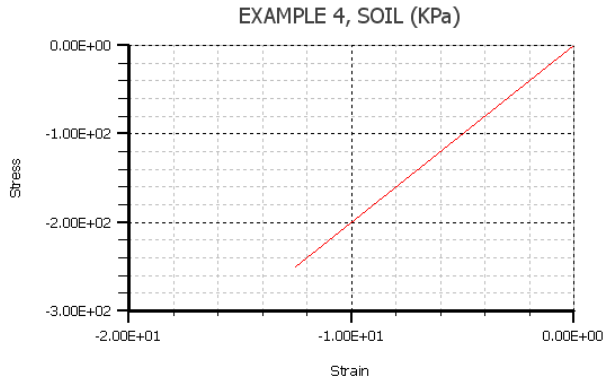

Fig. 9.4.2. Sand material in myBiAxial.

For an axial (compressive) load of $N_{Xc} = 1300kN$, the algorithm yields the following results: curvature $k = 4.807678$, precipitation at the origin $\varepsilon_c = 6.730731\text{mm}$, ultimate bending moment at failure $M_{Yc} = 4073.331kNm$. The failure occurs because the sand reaches the maximum stress capacity of 250KPa (fig. 9.4.3)

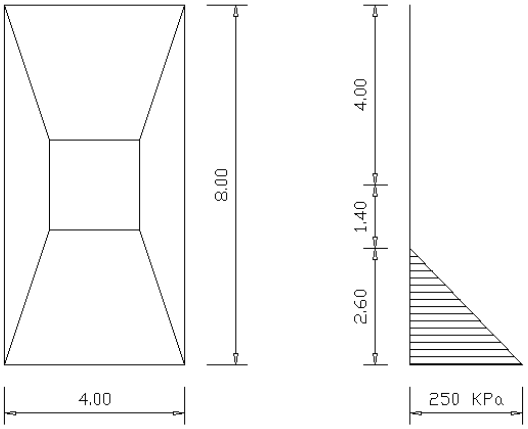

Fig. 9.4.3. Stress distribution.

The results are easily verifiable (eq. 9.4.1):

$$N = \frac{1}{2} \cdot 250KPa \cdot 2.60m \cdot 4.00m = 1300kN$$
$$M = 1300kN \cdot \left(1.40m + \frac{2}{3} \cdot 2.60m \right) = 4073.333kNm \tag{9.4.1}$$

As a step further, we may want to restrict the length of the ineffective area of the footing. This is achieved easily by applying a restriction similar to that of "Point C" of Eurocode 2, which is described in Example 1. For example, we demand that the settlement at distance $1/2 \cdot h$ from the most compressed point i.e. at the middle of the footing, to be less than or equal to zero. In this way, more than half of the footing is always in contact with the sand. In this case and for the same axial (compressive) load of $N_{Xc} = 1300kN$, the algorithm yields the following results: curvature $k = 2.031$, precipitation at the origin $\varepsilon_c = 0.00\text{mm}$, ultimate bending moment at failure $M_{Yc} = 3466.667kNm$.

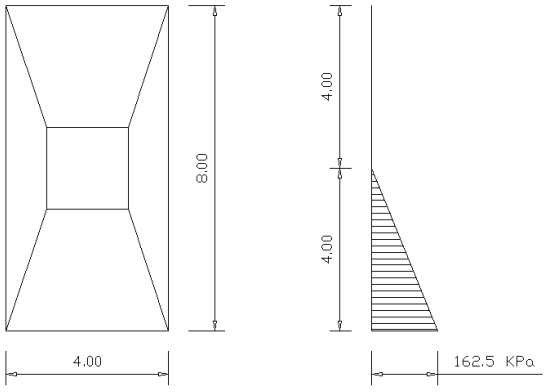

Fig. 9.4.4. Stress distribution.

The results are easily verifiable (eq. 9.4.2):

$$N = \frac{1}{2} \cdot 162.5KPa \cdot 4.00m \cdot 4.00m = 1300kN$$
$$M = 1300kN \cdot \left(\frac{2}{3} \cdot 4.00m \right) = 3466.666kNm \tag{9.4.2}$$

The complete interaction curve is shown in figure 9.4.5.

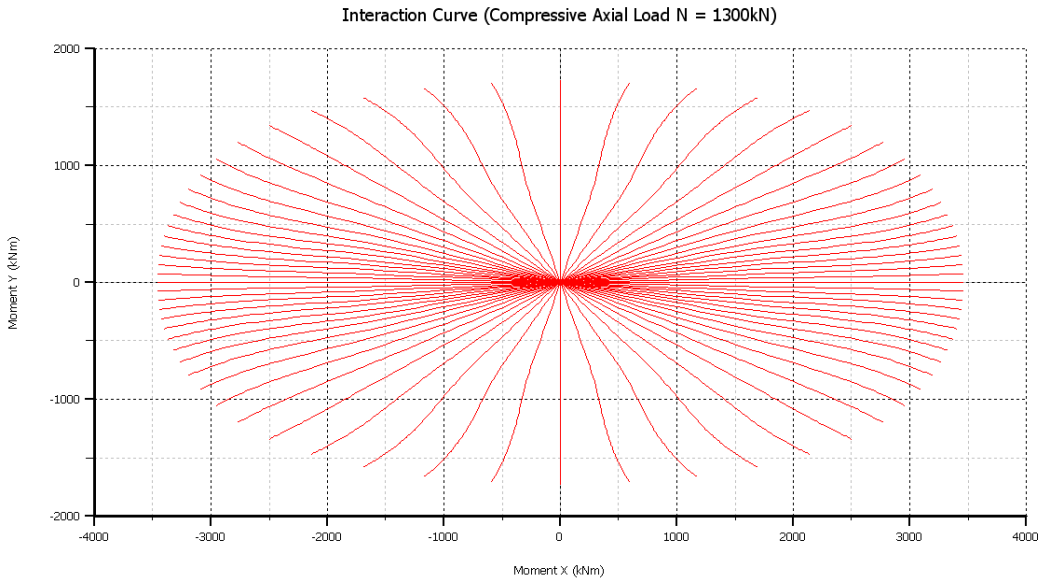

Fig. 9.4.5. Interaction curve for compressive axial load N = 1300kN.

10. References

1. Rodriguez, J. A., Aristizabal-Ochoa, J. Dario, *Biaxial interaction diagrams for short RC columns of any cross section*, J Struct Engng, ASCE 1999;125(6):672-683.
2. Rodriguez, J. A., Aristizabal-Ochoa, J. Dario, *M-P-φ diagrams for reinforced, partially and fully prestressed concrete sections under biaxial bending and axial load*, J Struct Engng, ASCE 2001;127(7):763-773.
3. Rodriguez, J. A., Aristizabal-Ochoa, J. Dario, *Reinforced, partially and fully prestressed concrete columns under biaxial bending and axial load*, J Struct Engng, ASCE 2001;127(7):774-783.
4. Chen, S. F., Teng, J. G., Chan, S. L., *Design of biaxially loaded short composite columns of arbitrary cross section*, J Struct Engng, ASCE 2001;127(6):678-685.
5. Sfakianakis, M. G., *Biaxial bending with axial force of reinforced, composite and repaired concrete sections of arbitrary shape by fiber model and computer graphics*, Advances in Engineering Software 33 (2002) 227 - 242.
6. Yen, J. Y. R., *Quasi-Newton method for reinforced concrete column analysis and design*, J Struct Engng, ASCE 1991;117(3):657-666.